PHYSICAL REVIEW B **86**, 075466 (2012)

Radiative heat transfer between neighboring particles

Alejandro Manjavacas* and F. Javier García de Abajo†
Instituto de Química Física "Rocasolano," Consejo Superior de Investigaciones Científicas, Serrano 119, 28006 Madrid, Spain
(Received 26 January 2012; revised manuscript received 10 June 2012; published 27 August 2012)

The near-field interaction between two neighboring particles is known to produce enhanced radiative heat transfer. We advance in the understanding of this phenomenon by including the full electromagnetic particle response, heat exchange with the environment, and important radiative corrections both in the distance dependence of the fields and in the particle absorption coefficients. We find that crossed terms of electric and magnetic interactions dominate the transfer rate between gold and SiC particles, whereas radiative corrections reduce it by several orders of magnitude even at small separations. Radiation away from the dimer can be strongly suppressed or enhanced at low and high temperatures, respectively. These effects must be taken into account for an accurate description of radiative heat transfer in nanostructured environments.

DOI: 10.1103/PhysRevB.86.075466 PACS number(s): 78.67.Bf, 44.40.+a, 12.20.Ds, 42.50.Lc

I. INTRODUCTION

Blackbody radiation mediates heat exchange between bodies placed in vacuum and separated by large distances d compared to the thermal wavelength $\lambda_T = 2\pi\hbar c/k_B T$. For parallel plates, this leads to a radiative heat transfer (RHT) rate independent of d. However, when $d \ll \lambda_T$, the rate is enhanced by several orders of magnitude due to the involvement of evanescent waves. Pioneering measurements[1,2] revealed this phenomenon, which was first explained in terms of near-field fluctuations.[3] After a long series of experimental[4,5] and theoretical[3,6–14] studies, recent observations have accurately confirmed a $1/d^2$ dependence for sapphire plates at room temperature down to $d \sim 1\,\mu$m,[5] and also a $1/d$ dependence for large silica spheres placed near a silica plate down to $d \sim 30$ nm,[15] although these laws can be substantially corrected by nonlocal,[11] phonon,[16,17] and photonic crystal[18] effects. In this context, the interaction of a particle with a plate has been explored both from experimental[4,15,19,20] and theoretical[12,16,21–24] fronts. Modeling heat exchange between two[25–31] or more[32] particles has been the subject of intense activity as well.

Magnetic polarization has been claimed to dominate RHT between metallic nanoparticles.[27] However, electromagnetic crossed terms (EMCTs, i.e., terms mixing the electric and magnetic particle responses) have been ignored so far, although they could play a leading role in transfers within heterogeneous structures. Likewise, radiative corrections in the absorption of dielectric particles deserve further consideration, as we show below. Thus, the current level of understanding of RHT between two particles appears to be incomplete.

Here, we formulate a complete solution of RHT between two nanoparticles within the assumption of dipolar response. We show that EMCTs are dominant in combinations of metallic and dielectric particles, such as gold and SiC. We introduce a relevant retardation correction beyond the customary treatment of polarization fluctuations, which results in a sizable reduction in the predicted transfer rate. Furthermore, we show that heat losses into the environment can be either dominant or negligible depending on the temperature and particle composition. An accurate description of RHT in nanostructured environments requires incorporating these effects, for which the two-particle system discussed here provides a tutorial approach as well as an estimate of the importance of EMCTs, radiative corrections, and interaction with the environment.

II. DESCRIPTION OF THE MODEL

We consider two spherical particles of radius R at temperatures T_1 and T_2 separated by a center-to-center distance d along the z direction and placed in a vacuum at temperature T_0, as shown in Fig. 1. We focus on small particles such that $R \ll d, \lambda_T$, so that their responses can be described through the polarizabilities α_1 and α_2 (see Ref. 26, Fig. 7, and Appendices A and B). RHT between the particles and the environment is produced by fluctuations in the vacuum electromagnetic field and the particle dipoles. We simplify the notation by combining electric and magnetic-field components acting on each particle $j = 1,2$, as well as electric (p) and magnetic (m) dipoles, in the vectors

$$E_j = \begin{pmatrix} E_{j,x} \\ E_{j,y} \\ E_{j,z} \\ H_{j,x} \\ H_{j,y} \\ H_{j,z} \end{pmatrix}, \quad p_j = \begin{pmatrix} p_{j,x} \\ p_{j,y} \\ p_{j,z} \\ m_{j,x} \\ m_{j,y} \\ m_{j,z} \end{pmatrix},$$

respectively. Likewise, the polarizability tensor becomes

$$\alpha_j = \begin{pmatrix} \alpha_j^E \mathbb{I}_3 & 0 \\ 0 & \alpha_j^M \mathbb{I}_3 \end{pmatrix},$$

where $\mathbb{I}_3$ is the 3×3 identity matrix and the E (M) subscript refers to electric (magnetic) components.

The net power absorbed by particle 1 is the sum of dipole and field fluctuation terms:

$$\mathcal{P}_1 = \mathcal{P}_1^{\text{field}} + \mathcal{P}_1^{\text{dip}}. \tag{1}$$

More precisely (see Appendix C),

$$P_1^{\text{field}} = \int_{-\infty}^{\infty} \frac{d\omega d\omega'}{(2\pi)^2} e^{-i(\omega-\omega')t}\, \omega' \langle E_1^+(\omega')[i\alpha^+(\omega') - (2k'^3/3)|\alpha(\omega')|^2] E_1(\omega)\rangle \tag{2}$$

represents the work exerted by the fluctuating field on particle 1. Here, $k = \omega/c$ is the wave vector of light at frequency ω.

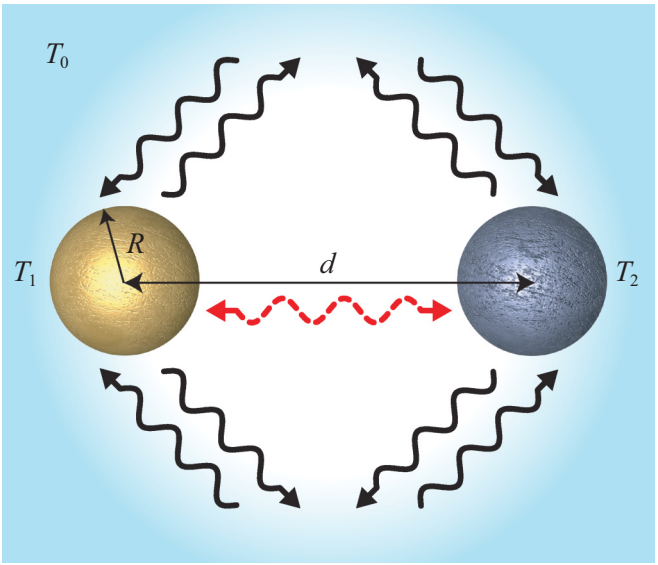

FIG. 1. (Color online) Description of the system under study. Two particles of radius R at temperatures T_1 and T_2 separated by a distance d are placed in a vacuum at temperature T_0. Each particle exchanges thermal energy with the other particle and with the surrounding vacuum.

Moreover, the self-consistent fields E_j include the response of the system to the fluctuating source fields $E_j^{\rm fl}$ via the relations

$$E_1 = E_1^{\rm fl} + \mathcal{G}_{12}\alpha_2 E_2, \quad E_2 = E_2^{\rm fl} + \mathcal{G}_{21}\alpha_1 E_1,$$

where $\mathcal{G}_{12}$ is the distance-dependent dipole-dipole interparticle interaction,

$$\mathcal{G}_{12} = \begin{pmatrix} A & 0 & 0 & 0 & -C & 0 \\ 0 & A & 0 & C & 0 & 0 \\ 0 & 0 & B & 0 & 0 & 0 \\ 0 & C & 0 & A & 0 & 0 \\ -C & 0 & 0 & 0 & A & 0 \\ 0 & 0 & 0 & 0 & 0 & B \end{pmatrix},$$

$$A = \exp(ikd)\,(k^2/d + ik/d^2 - 1/d^3),$$
$$B = \exp(ikd)\,2(1/d^3 - ik/d^2),$$
$$C = \exp(ikd)\,(k^2/d + ik/d^2),$$

and $\mathcal{G}_{21}$ takes the same form as $\mathcal{G}_{12}$ with C replaced by $-C$. In Eq. (2), $\langle\rangle$ represents the average over field fluctuations, which we perform by applying the fluctuation-dissipation theorem (FDT):[33,34]

$$\left\langle \left[E_j^{\rm fl}(\omega)\right]^+ E_{j'}^{\rm fl}(\omega')\right\rangle = 4\pi\hbar\delta(\omega-\omega')\eta_{jj'}(\omega)\left[n_0(\omega)+\tfrac{1}{2}\right],$$

where $\eta_{12} = (1/2)\,[{\rm Im}\{\mathcal{G}_{12}+\mathcal{G}_{21}\} + i{\rm Re}\{\mathcal{G}_{12}-\mathcal{G}_{21}\}]$, $\eta_{21} = \eta_{12}^+$, $\eta_{11} = \eta_{22} = (2k^3/3)\mathbb{I}_6$, and $n_0(\omega) = [\exp(\hbar\omega/k_BT_0) - 1]^{-1}$ is the Bose-Einstein distribution at the vacuum temperature T_0.

Likewise, the contribution of fluctuating dipoles is (see Appendix D)

$$P_1^{\rm dip} = \int_{-\infty}^{\infty} \frac{d\omega d\omega'}{(2\pi)^2} e^{-i(\omega-\omega')t}\left[i\omega'\langle p_1^+(\omega')\mathcal{G}_{12}(\omega)p_2(\omega)\rangle - \frac{2\omega^4}{3c^3}\langle p_1^+(\omega')p_1(\omega)\rangle\right], \quad (3)$$

where the first term inside the square brackets accounts for the effect of the field produced by particle 2 on particle 1, while the second term describes the interaction of the particle dipole with the vacuum. The self-consistent dipoles satisfy the relations

$$p_1 = p_1^{\rm fl} + \alpha_1\mathcal{G}_{12}p_2, \quad p_2 = p_2^{\rm fl} + \alpha_2\mathcal{G}_{21}p_1,$$

where $p_j^{\rm fl}$ is the fluctuating source dipole at particle j. The relevant FDT now becomes[33,34]

$$\left\langle \left[p_j^{\rm fl}(\omega)\right]^+ p_{j'}^{\rm fl}(\omega')\right\rangle = 4\pi\hbar\delta(\omega-\omega')\delta_{jj'}\chi_j(\omega)\left[n_j(\omega)+\tfrac{1}{2}\right],$$

where we use

$$\chi_j = {\rm Im}\{\alpha_j\} - (2k^3/3)|\alpha_j|^2\mathbb{I}_6, \quad (4)$$

rather than ${\rm Im}\{\alpha_j\}$, in order to prevent nonabsorbing particles from undergoing unphysical fluctuations. We set the polarizability to $\alpha_j^\nu = (3/2k^3)t_{j,1}^\nu$ ($\nu = E,M$), where $t_{j,1}^\nu$ is the dipole Mie scattering coefficient (see Appendix A). This definition of α_j complies with the optical theorem condition[35] ${\rm Im}\{\alpha_j\} \geqslant (2k^3/3)|\alpha_j|^2$, where the equality applies to nonabsorbing particles ($\chi_j = 0$). Incidentally, dipole and field fluctuations originate in different physical systems, and therefore there are not crossed terms between the two of them.

Finally, using the FDT to evaluate the integrals of Eqs. (2) and (3), we find, after some lengthy but straightforward algebra (see Appendix E),

$$\mathcal{P}_1 = \frac{2\hbar}{\pi}\sum_{\nu=E,M}\int_0^\infty \omega d\omega\ \chi_1^\nu \sum_{i=1}^{2}\left(\frac{2\Gamma_{i\perp}^\nu}{|s|^2} + \frac{\Gamma_{i\parallel}^\nu}{|t_\nu|^2}\right), \quad (5)$$

where

$$\Gamma_{1\perp}^\nu = \left[\frac{2k^3}{3}(|u_\nu|^2+|w_\nu|^2) + {\rm Im}\{\alpha_2^\nu[Au_\nu - g_\nu Cw_\nu] \times [Au_\nu^* + g_\nu Cw_\nu^*]\} + {\rm Im}\{\alpha_2^{\nu'} \times [Aw_\nu - g_\nu Cu_\nu][Aw_\nu^* + g_\nu Cu_\nu^*]\}\right](n_0-n_1),$$

$$\Gamma_{2\perp}^\nu = \left(\chi_2^\nu|Au_\nu - g_\nu Cw_\nu|^2 + \chi_2^{\nu'}|Aw_\nu - g_\nu Cu_\nu|^2\right)(n_2-n_0),$$

$$\Gamma_{1\parallel}^\nu = \left[\frac{2k^3}{3} + {\rm Im}\{\alpha_2^\nu B^2\}\right](n_0-n_1),$$

$$\Gamma_{2\parallel}^\nu = \chi_2^\nu|B|^2\,(n_2-n_0),$$

$$u_\nu = 1 - \alpha_1^{\nu'}\alpha_2^{\nu'}A^2 + \alpha_1^{\nu'}\alpha_2^\nu C^2,$$

$$w_\nu = \alpha_1^{\nu'}\left(\alpha_2^E - \alpha_2^M\right)AC,$$

$$s = 1 - \alpha_1^E\alpha_2^E A^2 - \alpha_1^M\alpha_2^M A^2 + \alpha_1^E\alpha_2^M C^2 + \alpha_1^M\alpha_2^E C^2 + \alpha_1^E\alpha_2^E\alpha_1^M\alpha_2^M(A^2-C^2)^2,$$

$$t_\nu = 1 - \alpha_1^\nu\alpha_2^\nu B^2,$$

and $\nu' = M$ (E) and $g_\nu = +1$ (-1) when $\nu = E$ (M).

Neglecting the magnetic response ($\alpha_j^M = 0$, $C = 0$), multiple scattering ($u_\nu = t_\nu = s = 1$, $w_\nu = 0$), and radiative corrections in the particles response ($\chi_j = {\rm Im}\{\alpha_j\}$), the above expressions reduce to

$$\mathcal{P}_1 = \frac{4\hbar}{\pi}\int_0^\infty \omega\, d\omega\ {\rm Im}\{\alpha_1^E\}\left\{\left[k^3 + 2{\rm Re}\{\alpha_2^E A\}{\rm Im}\{A\} + {\rm Re}\{\alpha_2^E B\}{\rm Im}\{B\}\right](n_0-n_1) + {\rm Im}\{\alpha_2^E\}(|A|^2 + |B|^2/2)\,(n_2-n_1)\right\},$$

where the $n_2 - n_1$ term describes direct RHT between the dimer particles and coincides with a previously reported expression.[25,27,30] The remaining $n_0 - n_1$ term accounts for heat exchange between particle 1 and the surrounding vacuum, partially assisted by the presence of particle 2.

III. RESULTS AND DISCUSSION

A. Heat transfer coefficient

We study in Figs. 2 and 3 the heat transfer coefficient (HTC) between two particles in a dimer when particle 1 is at the same temperature as the environment ($T_1 = T_0 = T$) and particle 2 is at a slightly different temperature ($T_2 = T + \delta T$). The HTC to particle 1 is defined per unit of temperature difference as $\mathcal{P}_1/\delta T$. Under these conditions, only the terms $\Gamma^{\nu}_{2,\perp}$ and $\Gamma^{\nu}_{2,\parallel}$ contribute to the transfer. The results obtained from the above formalism (solid curves) are compared to several approximations consisting of neglecting multiple scattering between the particles (circles, calculated for $u_\nu = t_\nu = s = 1$, $w_\nu = 0$), retardation effects everywhere (dashed curves, $k = 0$), retardation effects except in the particle response χ_j defined by Eq. (4) (triangles), or EMCTs (dotted curves).

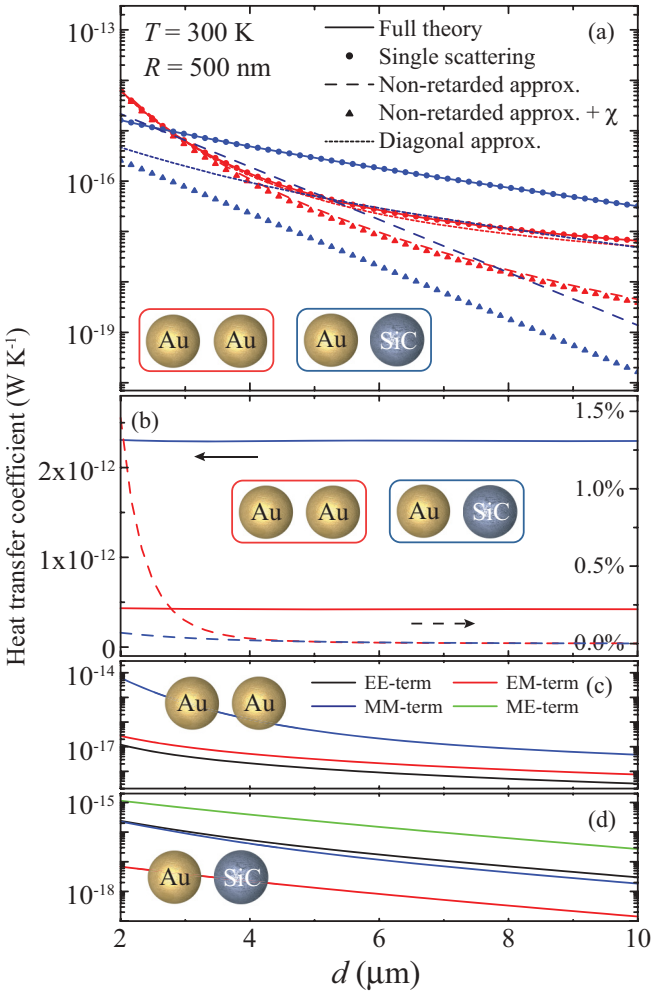

FIG. 2. (Color online) Dependence of the radiative heat transfer coefficient (HTC) on particle separation d. The HTC from particle 2 (right) to particle 1 (left) is defined as $\mathcal{P}_1/\delta T$ with $T_1 = T_0 = T$ and $T_2 = T + \delta T$ (see Fig. 1). (a) HTC at $T = 300$ K obtained from our full theory (solid curves), compared to the result of neglecting multiple scattering (circles), retardation effects everywhere (dashed curves), retardation effects except in χ_j (triangles), or EMCTs (dotted curves). Gold-gold (red curves) and gold-SiC (blue curves) dimers are considered. The particles radius is $R = 500$ nm. (b) Heat power lost by particle 2 (solid curves) and fraction of that power absorbed by particle 1 (broken curves, right scale). (c and d) Electric-electric (black), electric-magnetic (red), magnetic-magnetic (blue), and magnetic-electric (green) partial contributions to the HTC in the gold-gold (c) and gold-SiC (d) dimers.

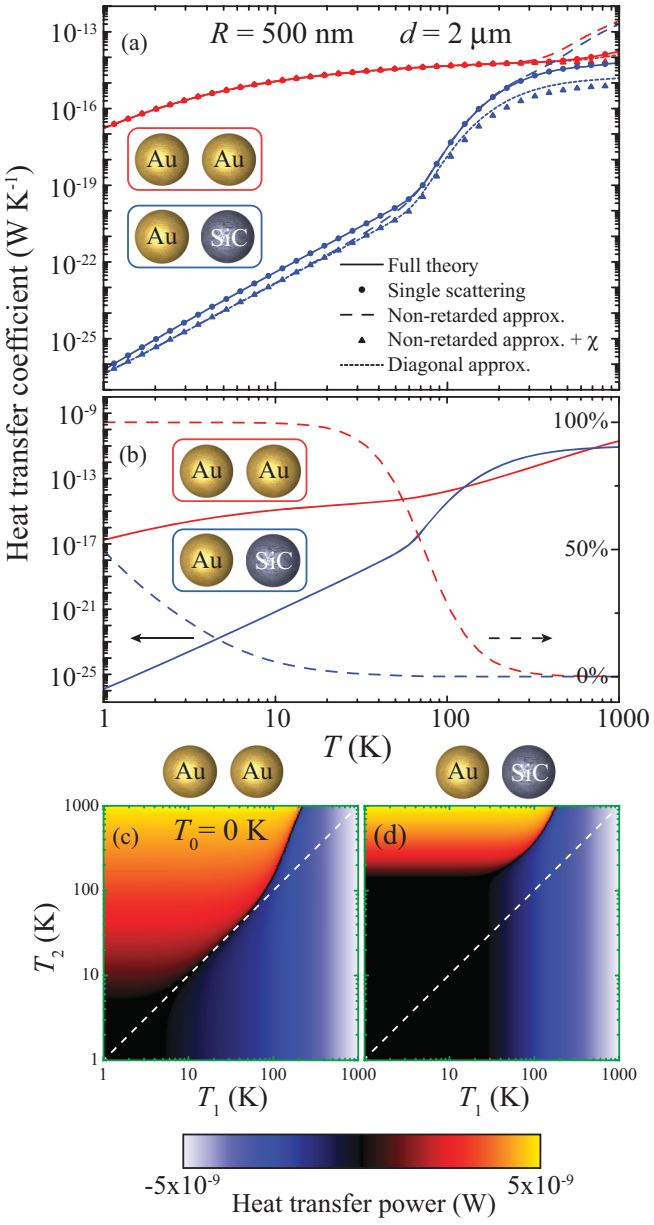

FIG. 3. (Color online) Temperature dependence of RHT. (a) HTC for the particles of Fig. 2. (b) Heat power lost by the right particle and fraction absorbed by the left particle. (c) Power absorbed (red-yellow scale, positive) or emitted (blue-white scale, negative) by the left particle of a gold-gold dimer as a function of T_1 and T_2 with the vacuum at $T_0 = 0$ (see Fig. 1). (d) Same as (c) for a gold-SiC dimer. The particle distance is $d = 2\,\mu$m and the radius is $R = 500$ nm in all cases.

B. Dependence on particle separation

The distance dependence of the HTC is analyzed in Fig. 2 for a homogeneous gold dimer and for a dimer formed by gold and SiC particles. As a first observation, we note that multiple scattering events can be safely neglected in all cases. In contrast, retardation causes a dramatic boost in the HTC, which increases with particle distance in both types of dimers. Additionally, the $|\alpha|^2$ term of Eq. (4) contributes with a uniform decreasing factor in SiC particles (see Fig. 7). (Notice that the absorption cross section is proportional to χ_j, whereas $\mathrm{Im}\{\alpha_j\}$ describes absorption plus scattering, so the $|\alpha|^2$ term in χ_j is removing scattering strength that is not associated with absorption.) Finally, EMCTs terms introduce additional channels of interparticle interaction, thus resulting in higher transfer rates compared to the diagonal approximation (consisting of only including electric-electric and magnetic-magnetic terms), particularly in the heterogeneous dimer [Fig. 2(a)]. Figure 2(c) clearly shows that the magnetic-magnetic terms are dominant in the homogeneous gold dimer, in agreement with previous predictions,[27] because metallic particles mainly contribute through magnetic polarization. This is unlike the heterogeneous cluster, in which magnetic-electric terms are dominant [Fig. 2(d)], thus picking up an important electric polarization from the SiC particle. Incidentally, the HTCs from gold to SiC and from SiC to gold are nearly identical (see Fig. 4).

C. Temperature dependence

Similar conclusions are extracted from the temperature dependence of the HTC, represented in Fig. 3(a) for a small distance $d = 2\,\mu\mathrm{m} \ll \lambda_T = 14\,\mu\mathrm{m}-14$ mm. Notice however the dramatic reduction in the transfer rate produced by retardation at high temperatures. This behavior can be understood from the spectral dependence exhibited by the integrand of Eq. (5) (see Fig. 6).

Incidentally, we are considering particle temperatures up to ∼1000 K, for which the permittivities of the materials under discussion should only undergo minor thermal effects, certainly indiscernible on the logarithmic scales of the figures. Thermal effects can change the permittivity by producing volume expansion, and thus a reduction of the conduction-electron density, and also by altering the Fermi distribution near the Fermi level E_F in metals. Both of these effects are small, and in particular we have $k_B T \ll E_F$.

The full dependence on the particle temperatures for a vacuum at $T_0 = 0$ is studied in Figs. 3(c) and 3(d). Interestingly, particle 1 gets cooled down (blue regions) even if particle 2 is at a higher temperature. This is due to radiation losses into the vacuum. However, particle 2 in the homogeneous cluster is rather efficient in transferring energy to particle 1 and compensating for radiation losses, so that the curve separating gains (red) from losses (blue) is closer to the $T_1 = T_2$ line (dashed) in that dimer [Fig. 3(c)].

D. Radiation emission

An important ingredient that is often overlooked in the analysis of heat transfer relates to how much energy is emitted into the surrounding vacuum. We analyze this in Figs. 2(b) and 3(b) by calculating the power escaping from a hotter particle 2. The calculation is done by reversing the particle

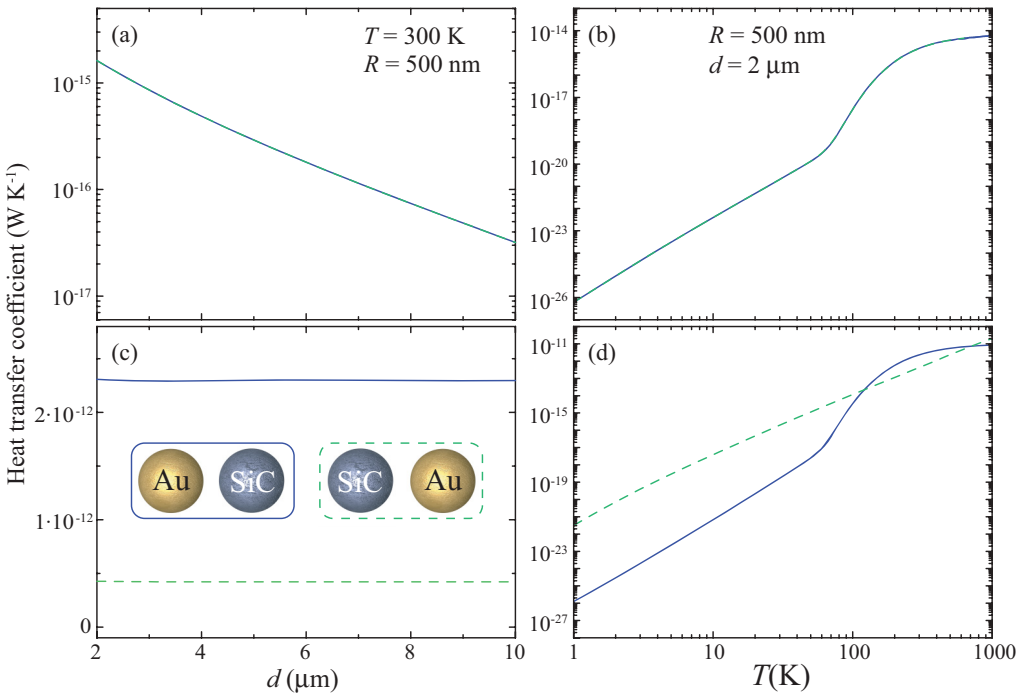

FIG. 4. (Color online) (a and b) Heat transfer coefficient (HTC) as a function of particle distance d and temperature T for a gold-SiC dimer (solid curves) and a SiC-gold dimer (broken curves). The HTC from the right particle 2 to the left particle 1 is defined as $\mathcal{P}_1/\delta T$ [see Eq. (E1)] with $T_1 = T_0 = T$ and $T_2 = T + \delta T$ [see insets in (c) for sketches of the dimers]. (c and d) Power emanating from the right particle in the two dimer orientations under consideration.

labels, so that only the terms $\Gamma^{\nu}_{1,\perp}$ and $\Gamma^{\nu}_{1,\parallel}$ contribute in this case [see Eq. (5)]. For the temperature of Fig. 2, just a small amount of the energy emanating from particle 2 ends up in particle 1. However, this fraction increases at lower temperatures [Figs. 3(b)], until nearly complete heat transfer takes place below ∼10 K in the homogeneous gold dimer. The fraction of heat transferred between the particles is thus very sensitive to temperature and particle distance (see Fig. 5).

E. Symmetric and asymmetric heat transfers in inhomogeneous dimers

We show in Figs. 4(a) and 4(b) the different heat transfer coefficients (HTCs) exhibited by an inhomogeneous gold-SiC dimer when the hotter particle is either SiC (solid curves) or gold (dashed curves) and the transfer is for heat absorbed by the remaining gold or SiC particle, respectively. The power transfer to the cooler particle is nearly independent of whether the hotter particle is SiC or Au. This symmetry upon permutation of particle indices ($1 \leftrightarrow 2$) is complete if we neglect multiple scattering between the particles [i.e., by setting $u_\nu = 1$ and $w_\nu = 0$ in Eq. (5), since only $\Gamma^{\nu}_{2,\perp}$ and $\Gamma^{\nu}_{2\parallel}$ terms contribute to the HTC], and indeed multiple scattering can be neglected in the clusters under consideration, as shown in Figs. 2 and 3.

In contrast, the total heat lost by the hotter particle is strongly dependent on whether this is gold or SiC [see Figs. 4(c) and 4(d)]. Part of this heat is absorbed by the cooler particle, but the rest is radiated into the surrounding vacuum. At high temperatures above ∼100 K, a hotter SiC particle produces larger radiation rates [Fig. 4(d)], rather independent of particle distance [Fig. 4(c)]. However, hotter gold is more capable of radiating at smaller temperatures [cf. vertical scales in Figs. 4(b) and 4(d)].

F. Total rate of heat loss and fraction of power exchange

Heat exchange with the surrounding vacuum plays a leading role in the energy balance during radiative thermalization of a particle dimer, as shown in Fig. 5. We plot in Fig. 5(a) the power lost by the right particle when it is placed at a slightly higher temperature with respect to both the vacuum and the left particle (i.e., we represent $-\mathcal{P}_2/\delta T$ for $T_0 = T_1 = T$ and $T_2 = T + \delta T$). At high temperatures, this power is rather insensitive to the presence of the neighboring particle and no significant dependence on particle separation d is observed. This happens above $T \sim 50$ K in the inhomogeneous gold-SiC dimer and above $T \sim 300$ K in the homogeneous gold-gold dimer. However, the accompanying left particle has a strong influence on the power loss of the right particle at lower temperatures, especially in the homogeneous dimer. The power loss increases when the particles are placed closer together. We show next that this is partially explained by the effect of additional absorption by the left particle.

Figure 5(b) shows the fraction of the power lost by the right particle that is absorbed by the left particle. This fraction drops to small values at large temperatures, but it eventually approaches 100% at lower temperatures. This behavior is consistent with the distance dependence of the power lost by the right particle. Nearly full radiative heat transfer between two neighboring particles with negligible radiation into the surrounded vacuum is thus possible at sufficiently low temperatures. Specifically, in the gold-gold dimer this regime is already achieved at ∼100 K for particles of radius $R = 500$ nm and a surface-to-surface separation of one radius (i.e., $d = 1.5\,\mu$m). We observe that the temperature below which nearly 100% transfer between the dimer particles takes place decreases with increasing separation.

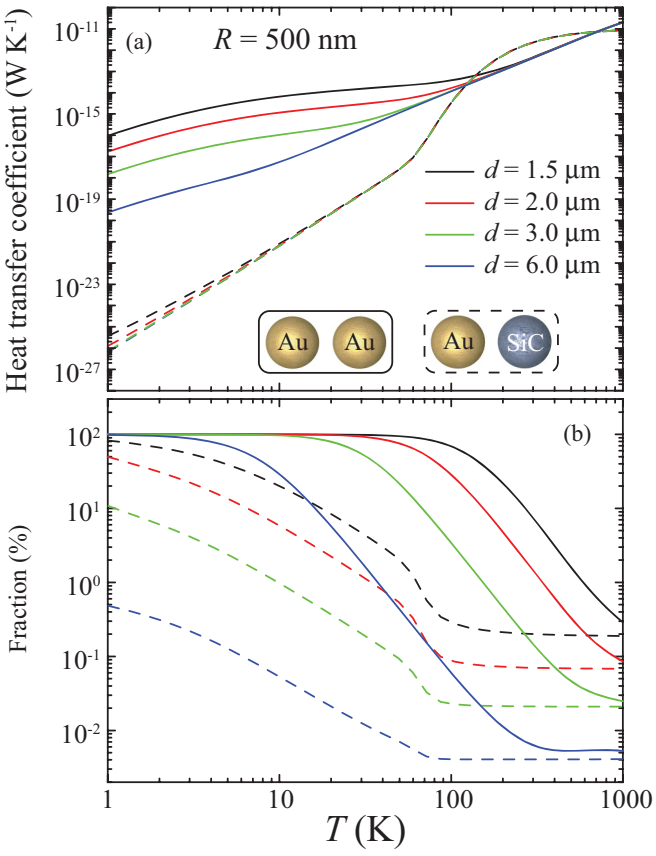

FIG. 5. (Color online) (a) Heat power lost by the right particle as a function of temperature for different particle separations. The right particle is slightly hotter than both the vacuum and the left particle, which are prepared at the same temperature, and the rate is normalized to the small temperature difference of the right particle (i.e., we represent $-\mathcal{P}_2/\delta T$ for $T_0 = T_1 = T$ and $T_2 = T + \delta T$). (b) Fraction of the power lost by the right particle that ends up being absorbed by the left particle.

G. Spectral dependence of radiative heat transfer

It is useful to analyze the spectral contribution from different photon energies to the HTC [i.e., the integrand of Eq. (5)]. At a low temperature $T = 10$ K [Fig. 6(a)], the exchange is dominated by low photon energies, for which the particle polarizations show a featureless behavior and χ_j almost coincides with $\mathrm{Im}\{\alpha_j\}$ for the size of the particles under discussion (see Fig. 7). At high temperature $T = 1000$ K [Fig. 6(b)], optical phonons emerge as a sharp infrared (IR) feature in SiC and plasmons show up as a broader near-IR feature in gold particles. Retardation effects also increase with T, as the particles appear to be large in front of λ_T.

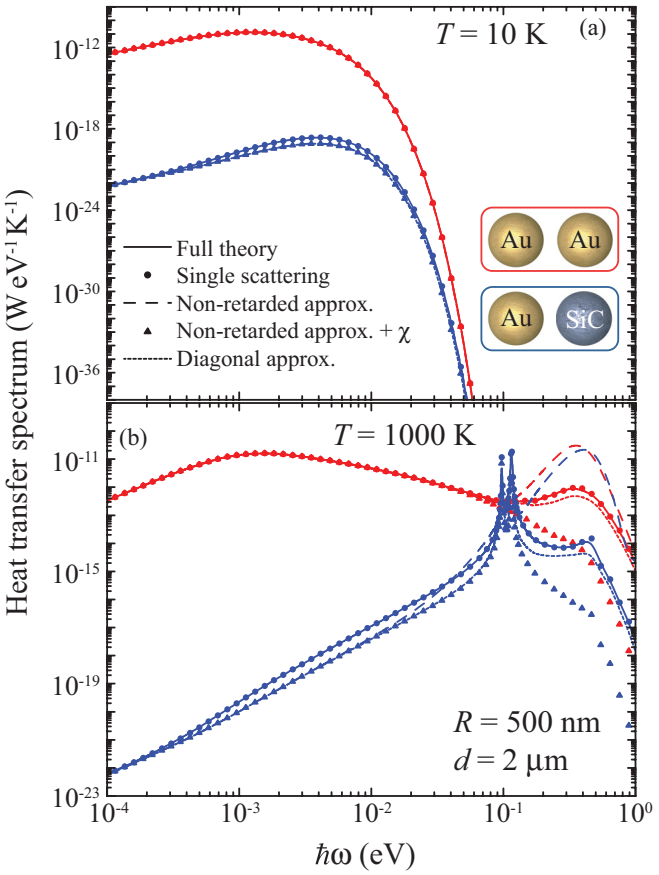

FIG. 6. (Color online) Spectral dependence of the radiative HTC for two different temperatures (see labels), obtained from our full theory (solid curves), compared to the result of neglecting multiple scattering (circles), retardation effects everywhere (dashed curves), retardation effects except in χ_j (triangles), or EMCTs (dotted curves). Gold-gold (red curves) and gold-SiC (blue curves) dimers are considered. The radius of the particles is $R = 500$ nm and their separation is $d = 2\,\mu$m. Notice that the range of validity of the dipolar approximation is limited by contributions coming from multipolar terms, as discussed in Fig. 8.

IV. CONCLUSIONS

Heat dissipation in nanostructured devices is becoming a limiting factor in the design of microchips and is expected to play a major role in nanoelectronics, nanophotonics, and photovoltaics. Radiative losses provide a convenient way of handling the excess of heat produced in these devices.[36] In this context, crossed magnetic-electric terms and radiative corrections as those described here produce modifications in the transfer rate by up to several orders of magnitude, which cannot be overlooked. An analysis of how much heat is released from a dimer into a cooler vacuum reveals a large dependence on composition and temperature (it is strongly suppressed at low temperatures and dominant in hot environments). Our results for gold-SiC dimers suggest the experimental exploration of these effects via, for example, in-vacuum particle levitation or by attaching one of the particles to a nanoscale tip and the other one to an insulating substrate. As an interesting direction, we note that RHT can be strongly modified by the presence of additional mirrors and dielectrics that distort the exchanged electromagnetic fields. We further suggest the possibility of molding RHT down to the quantum regime by placing the particles in a resonant cavity. This directly connects to the proposed quantization of RHT,[37] similar to that observed in the conventional thermal conductance of narrow bridges.[38]

ACKNOWLEDGMENTS

This work has been supported by the Spanish Ministry of Science and Innovation (MAT2010-14885 and Consolider NanoLight.es) and the European Commission (FP7-ICT-2009-4-248909-LIMA and FP7-ICT-2009-4-248855-N4E). A.M. acknowledges financial support through FPU from ME.

APPENDIX A: PARTICLE POLARIZABILITY

We obtain the polarizability of the homogeneous spherical particles under consideration from their dipolar Mie scattering coefficients as $\alpha_j^\nu = (3/2k^3)t_{j,1}^\nu$ ($\nu = E, M$), where $k = \omega/c$. This procedure automatically incorporates retardation corrections in the polarizability. The Mie coefficients are given by the analytical expressions[39]

$$t_l^M = \frac{-j_l(\rho_0)\rho_1 j_l'(\rho_1) + \rho_0 j_l'(\rho_0) j_l(\rho_1)}{h_l^{(+)}(\rho_0)\rho_1 j_l'(\rho_1) - \rho_0 [h_l^{(+)}(\rho_0)]' j_l(\rho_1)},$$

$$t_l^E = \frac{-j_l(\rho_0)[\rho_1 j_l(\rho_1)]' + \epsilon[\rho_0 j_l(\rho_0)]' j_l(\rho_1)}{h_l^{(+)}(\rho_0)[\rho_1 j_l(\rho_1)]' - \epsilon[\rho_0 h_l^{(+)}(\rho_0)]' j_l(\rho_1)},$$

where $\rho_0 = kR$, $\rho_1 = kR\sqrt{\epsilon}$ with $\mathrm{Im}\{\rho_1\} > 0$, R is the particle radius, ϵ is its dielectric function, j_l and $h_l^{(+)} = i h_l^{(1)}$ are spherical Bessel and Hankel functions, and the prime denotes differentiation with respect to ρ_0 and ρ_1.

Figure 7 shows the imaginary part of the particle polarizability $\mathrm{Im}\{\alpha\}$ compared with the absorption factor $\chi = \mathrm{Im}\{\alpha\} - 2k^3/3|\alpha|^2$ for gold and SiC spheres of radius R similar to those considered in Sec. III. As expected, χ approaches $\mathrm{Im}\{\alpha\}$ in the $kR \ll 1$ limit (i.e., when retardation is negligible). However, $\mathrm{Im}\{\alpha\}$ and χ behave increasingly different as the energy goes up. The difference between these two functions increases with particle size, or equivalently the threshold for retardation effects $\omega \approx c/R$ (e.g., 0.4 eV for $R = 500$ nm) is lowered. Interestingly, the magnetic (electric) component is dominant in gold (SiC) particles at energies below ~0.1 eV, while plasmon (phonon) resonances take over for larger ω.

APPENDIX B: VALIDITY OF THE DIPOLAR APPROXIMATION

The dipolar approximation should be accurate in the limit of small particles compared with the light wavelength. The validity of this approximation is tested in Fig. 8 by comparing the extinction cross-section of gold dimers calculated by representing the particles as dipoles (broken curves) or by including all multipoles (solid curves). The calculations are performed using a multiple elastic scattering of multipolar expansions (MESME) method.[39] We obtain similar values of the cross section in both calculations for different particle separations down to $d = 1.5\,\mu$m when the photon energy is

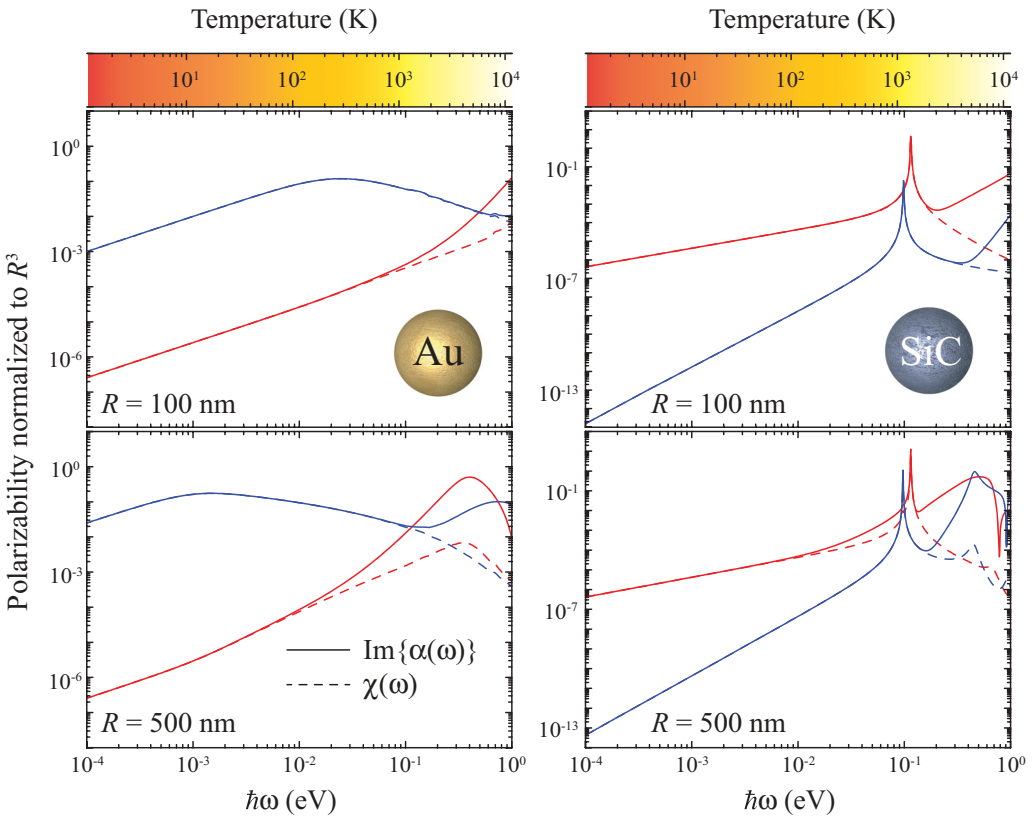

FIG. 7. (Color online) Imaginary part of the polarizability $\mathrm{Im}\{\alpha^\nu\}$ (solid curves) and absorption coefficient $\chi^\nu = \mathrm{Im}\{\alpha^\nu\} - (2k^3/3)|\alpha^\nu|^2$ (dashed curves) for gold (a and b) and SiC (c and d) spherical particles of different radius R, as a function of photon energy. Red and blue curves represent electric ($\nu = E$) and magnetic ($\nu = M$) components. The upper color scale shows the equivalent temperature $\hbar\omega/k_B$. Notice that the range of validity of the dipolar approximation is limited by contributions coming from multipolar terms, as discussed in Fig. 8.

smaller than $\hbar c/R \approx 0.4$ eV, where $R = 500$ nm is the particle radius. The complex plasmon features showing up at larger energies in the full calculation are not captured within the dipolar approximation. Our formalism is thus appropriate to describe dimers within this range of sizes and separations for temperatures below $\sim \hbar c/k_B R \approx 4580$ K.

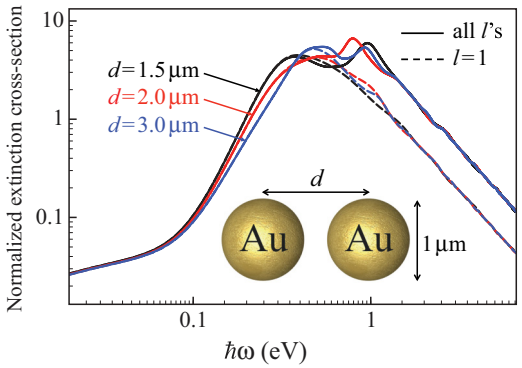

FIG. 8. (Color online) Extinction cross-section spectra of gold dimers calculated in the dipolar approximation ($l = 1$, dashed curves) and with full inclusion of all multipoles (solid curves) for different distances between particle centers d, as indicated by labels. The particles diameter is 1 μm. The cross section is normalized to the projected area of one particle.

APPENDIX C: DERIVATION OF EQ. (2)

We consider a spherical particle placed at the origin and of radius much smaller than the thermal wavelength $\lambda_T = 2\pi\hbar c/k_B T$ [see Fig. 9(a)], so that it can be described by its electric and magnetic polarizabilities, α^E and α^M, respectively. Under illumination by an external electromagnetic plane wave of frequency ω and wave vector $\mathbf{k}$, the total field (external plus induced) can be written

$$\mathbf{E}(\mathbf{r},t) = \mathbf{E}_0 e^{i\mathbf{k}\cdot\mathbf{r}} e^{-i\omega t} + \mathcal{G}(\mathbf{r},\omega)\alpha^{\mathrm{E}}(\omega)\mathbf{E}_0 e^{-i\omega t} - \frac{1}{ik}\nabla\times\mathcal{G}(\mathbf{r},\omega)\alpha^{\mathrm{M}}(\omega)\mathbf{H}_0 e^{-i\omega t} + \mathrm{c.c.}, \quad \text{(C1a)}$$

$$\mathbf{H}(\mathbf{r},t) = \mathbf{H}_0 e^{i\mathbf{k}\cdot\mathbf{r}} e^{-i\omega t} + \mathcal{G}(\mathbf{r},\omega)\alpha^{\mathrm{M}}(\omega)\mathbf{H}_0 e^{-i\omega t} + \frac{1}{ik}\nabla\times\mathcal{G}(\mathbf{r},\omega)\alpha^{\mathrm{E}}(\omega)\mathbf{E}_0 e^{-i\omega t} + \mathrm{c.c.}, \quad \text{(C1b)}$$

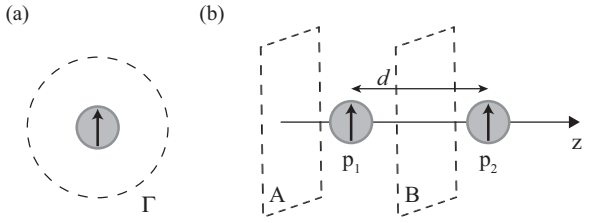

FIG. 9. Description of the geometry used in the derivation of Eqs. (2) and (3).

where

$$\mathcal{G}(\mathbf{r},\omega) = [k^2 + \nabla \otimes \nabla]\frac{e^{ikr}}{r} \tag{C2}$$

is the electromagnetic Green tensor. The work exerted on the particle by the external electromagnetic field can be obtained from the Poynting vector flux across a spherical surface S of radius r centered at the origin as

$$\mathcal{P}_1^{\text{field}} = \frac{c}{4\pi} r^2 \int_S d\Omega\, [\mathbf{E}(\mathbf{r},t) \times \mathbf{H}(\mathbf{r},t)] \cdot \hat{\mathbf{r}}. \tag{C3}$$

Now, inserting Eqs. (C1) into Eq. (C3), we readily obtain the expression

$$\mathcal{P}_1^{\text{field}} = \omega\left[-i\alpha^{\text{E}} - \frac{2k^3}{3}|\alpha^{\text{E}}|^2\right]|\mathbf{E}_0|^2 + \omega\left[-i\alpha^{\text{M}} - \frac{2k^3}{3}|\alpha^{\text{M}}|^2\right]|\mathbf{H}_0|^2 + \text{c.c.}, \tag{C4}$$

where we have only retained stationary terms. Equation (C4) is the monochromatic version of Eq. (2).

APPENDIX D: DERIVATION OF EQ. (3)

We now consider two neighboring spherical particles placed at the origin and at a distance d from the origin along the z axis, respectively, as shown in Fig. 9(b). We assume small particles compared to both λ_T and d, so that we can describe them as point electric and magnetic dipoles, $\mathbf{p}_j$ and $\mathbf{m}_j$, respectively, where $j = 1,2$ labels the particles. We calculate the power absorbed by particle 1 from the Poynting vector flux in the direction towards the particle across two infinite planes A and B normal to $\hat{\mathbf{z}}$, as shown in Fig. 9(b). More precisely,

$$\mathcal{P}_1^{\text{dip}} = \frac{c}{4\pi}\left(\int_A - \int_B\right) d\mathbf{R}\, [\mathbf{E}(\mathbf{r},t) \times \mathbf{H}(\mathbf{r},t)] \cdot \hat{\mathbf{z}}. \tag{D1}$$

Taking advantage of this geometry, the electromagnetic field created by the electric and magnetic particle dipoles can be written

$$\mathbf{E}(\mathbf{r},t) = \frac{ie^{-i\omega t}}{2\pi}\sum_{i=1,2}\int \frac{d\mathbf{Q}}{q}[(k^2 + \nabla \otimes \nabla)\mathbf{p}_i + ik\nabla \times \mathbf{m}_i]e^{i\mathbf{Q}\cdot\mathbf{R}}e^{iq|z-z_i|} + \text{c.c.}, \tag{D2a}$$

$$\mathbf{H}(\mathbf{r},t) = \frac{ie^{-i\omega t}}{2\pi}\sum_{i=1,2}\int \frac{d\mathbf{Q}}{q}[(k^2 + \nabla \otimes \nabla)\mathbf{m}_i - ik\nabla \times \mathbf{p}_i]e^{i\mathbf{Q}\cdot\mathbf{R}}e^{iq|z-z_i|} + \text{c.c.}, \tag{D2b}$$

where we have used the relation

$$\frac{e^{ikr}}{r} = \frac{i}{2\pi}\int \frac{d\mathbf{Q}}{q} e^{i\mathbf{Q}\cdot\mathbf{R}} e^{iq|z-z_i|},$$

the integrals are extended over wave vectors along x and y directions, and $q = \sqrt{k^2 - Q^2}$ ($q = i\sqrt{Q^2 - k^2}$) is the wave vector along z for $k \geqslant Q$ ($k < Q$). Finally, inserting Eqs. (D2) into Eq. (D1) we obtain, after some straightforward algebra,

$$\begin{aligned}\mathcal{P}_1^{\text{dip}} = {} & i\omega A(p_{1x}^* p_{2x} + p_{1y}^* p_{2y} + m_{1x}^* m_{2x} + m_{1y}^* m_{2y}) \\ & + i\omega B(p_{1z}^* p_{2z} + m_{1z}^* m_{2z}) \\ & + i\omega C(-p_{1x}^* m_{2y} + p_{1y}^* m_{2x} + m_{1x}^* p_{2y} - m_{1y}^* p_{2x}) \\ & - \frac{2\omega^4}{3c^3}(|\mathbf{p}_1|^2 + |\mathbf{m}_1|^2) + \text{c.c.},\end{aligned}$$

which is the monochromatic version of Eq. (3), where A, B, and C are defined in Sec. II.

APPENDIX E: DERIVATION OF EQ. (5)

We follow the notation and definitions introduced in Fig. 1 for the system under consideration. The net power absorbed by particle 1 can be written as shown in Eq. (1).

Now, using the expressions for the self-consistent fields and dipoles (see Sec. II)

$$\begin{aligned} E_1 &= D^{-1}\left[E_1^{\text{fl}} + \mathcal{G}_{12}\alpha_2 E_2^{\text{fl}}\right], \\ p_1 &= D_1^{-1}\left[p_1^{\text{fl}} + \alpha_1\mathcal{G}_{12}p_2^{\text{fl}}\right], \\ p_2 &= D_2^{-1}\left[p_2^{\text{fl}} + \alpha_2\mathcal{G}_{21}p_1^{\text{fl}}\right], \end{aligned}$$

where the denominators $D = \mathbb{I}_3 - \mathcal{G}_{12}\alpha_2\mathcal{G}_{21}\alpha_1$, $D_1 = \mathbb{I}_3 - \alpha_1\mathcal{G}_{12}\alpha_2\mathcal{G}_{21}$, and $D_2 = \mathbb{I}_3 - \alpha_2\mathcal{G}_{21}\alpha_1\mathcal{G}_{12}$ describe multiple scattering, Eq. (1) becomes

$$\begin{aligned}\mathcal{P}_1 = {} & \int_{-\infty}^{\infty}\frac{d\omega d\omega'}{(2\pi)^2}e^{-i(\omega-\omega')t}\left\{\omega'\left[\left\langle E_1^{\text{fl}+}(D^{-1})^+[i\alpha^+ - (2k^3/3)|\alpha|^2]D^{-1}E_1^{\text{fl}}\right\rangle + \left\langle E_1^{\text{fl}+}(D^{-1})^+[i\alpha^+ - (2k^3/3)|\alpha|^2]D^{-1}\mathcal{G}_{12}\alpha_2 E_2^{\text{fl}}\right\rangle\right.\right. \\ & \left.\left. + \left\langle E_2^{\text{fl}+}\alpha_2^+\mathcal{G}_{12}^+(D^{-1})^+[i\alpha^+ - (2k^3/3)|\alpha|^2]D^{-1}E_1^{\text{fl}}\right\rangle + \left\langle E_2^{\text{fl}+}\alpha_2^+\mathcal{G}_{12}^+(D^{-1})^+[i\alpha^+ - (2k^3/3)|\alpha|^2]D^{-1}\mathcal{G}_{12}\alpha_2 E_2^{\text{fl}}\right\rangle\right] \\ & + \left[i\omega'\left\langle p_1^{\text{fl}+}(D_1^{-1})^+\mathcal{G}_{12}D_2^{-1}\alpha_2\mathcal{G}_{21}p_1^{\text{fl}}\right\rangle + i\omega'\left\langle p_2^{\text{fl}+}\mathcal{G}_{12}^+\alpha_1^+(D_1^{-1})^+\mathcal{G}_{12}D_2^{-1}p_2^{\text{fl}}\right\rangle - \frac{2\omega^4}{3c^3}\left\langle p_1^{\text{fl}+}|D_1|^{-2}p_1^{\text{fl}}\right\rangle\right. \\ & \left.\left. - \frac{2\omega^4}{3c^3}\left\langle p_2^{\text{fl}+}\mathcal{G}_{12}^+\alpha_1^+|D_1|^{-2}\alpha_1\mathcal{G}_{12}p_2^{\text{fl}}\right\rangle\right]\right\} = \sum_{j=1}^{8} I_j.\end{aligned}$$

We then carry out the matrix multiplications in this expression and apply the FDT. After some algebra, we find

$$I_1 = \frac{\hbar}{\pi}\int_0^{\infty} d\omega \frac{4}{3}\omega k^3 \sum_{\nu=E,M}\chi_1^{\nu}\left[2\left|\frac{u_\nu}{s}\right|^2 + 2\left|\frac{w_\nu}{s}\right|^2 + \left|\frac{1}{t_\nu}\right|^2\right]\left(n_0 + \frac{1}{2}\right),$$

$$I_2+I_3=\frac{\hbar}{\pi}\int_0^\infty d\omega 8\omega\sum_{\nu=E,M}\chi_1^\nu\Bigg[\mathrm{Re}\Bigg\{\alpha_2^\nu A\left|\frac{u_\nu}{s}\right|^2-g_\nu\alpha_2^\nu C\frac{u_\nu^*w_\nu}{|s|^2}-g_\nu\alpha_2^{\nu'}C\frac{u_\nu w_\nu^*}{|s|^2}+\alpha_2^{\nu'}A\left|\frac{w_\nu}{s}\right|^2\Bigg\}\mathrm{Im}\{A\}$$
$$-\mathrm{Im}\Bigg\{\alpha_2^\nu C\left|\frac{w_\nu}{s}\right|^2-g_\nu\alpha_2^\nu A\frac{u_\nu w_\nu^*}{|s|^2}-g_\nu\alpha_2^{\nu'}A\frac{u_\nu^*w_\nu}{|s|^2}+\alpha_2^{\nu'}A\left|\frac{u_\nu}{s}\right|^2\Bigg\}\mathrm{Re}\{C\}+\frac{1}{2}\mathrm{Re}\Bigg\{\alpha_2^\nu B\left|\frac{1}{t_\nu}\right|^2\Bigg\}\mathrm{Im}\{B\}\Bigg]\left(n_0+\frac{1}{2}\right),$$

$$I_4=\frac{\hbar}{\pi}\int_0^\infty d\omega\frac{4}{3}\omega k^3\sum_{\nu=E,M}\chi_1^\nu\left[2\left|\alpha_2^\nu\right|^2\left|A\frac{u_\nu}{s}-g_\nu C\frac{w_\nu}{s}\right|^2+2\left|\alpha_2^{\nu'}\right|^2\left|A\frac{w_\nu}{s}-g_\nu C\frac{u_\nu}{s}\right|^2+\left|\alpha_2^\nu\right|^2\left|\frac{B}{t_\nu}\right|^2\right]\left(n_0+\frac{1}{2}\right),$$

$$I_5=\frac{\hbar}{\pi}\int_0^\infty d\omega 4\omega\sum_{\nu=E,M}\chi_1^\nu\mathrm{Im}\Bigg\{\frac{\alpha_2^\nu}{|s|^2}[-A^2|u_\nu|^2+g_\nu ACu_\nu^*w_\nu-g_\nu ACu_\nu w_\nu^*+A^2|w_\nu|^2]+\frac{\alpha_2^{\nu'}}{|s|^2}[C^2|u_\nu|^2-g_\nu ACu_\nu^*w_\nu$$
$$+g_\nu ACu_\nu w_\nu^*-C^2|w_\nu|^2]-\frac{1}{2}\alpha_2^\nu B^2\left|\frac{1}{t_\nu}\right|^2-\frac{w_\nu^*}{|s|^2}\left[\alpha_2^\nu\left(\alpha_1^{\mathrm{E}}\alpha_2^{\mathrm{M}}-\alpha_2^{\mathrm{E}}\alpha_1^{\mathrm{M}}\right)-\alpha_2^{\nu'}\left(\alpha_1^{\mathrm{E}}\alpha_2^{\mathrm{E}}-\alpha_1^{\mathrm{M}}\alpha_2^{\mathrm{M}}\right)\right](AC^3-A^3C)\Bigg\}\left(n_1+\frac{1}{2}\right),$$

$$I_6=\frac{\hbar}{\pi}\int_0^\infty d\omega 4\omega\sum_{\nu=E,M}\chi_1^\nu\mathrm{Im}\Bigg\{\frac{\alpha_2^\nu}{|s|^2}\left[|Au_\nu|^2+g_\nu AC^*u_\nu^*w_\nu-g_\nu AC^*u_\nu w_\nu^*-|Aw_\nu|^2\right]+\frac{\alpha_2^{\nu'}}{|s|^2}\left[|Cu_{\nu'}|^2-g_\nu A^*Cu_{\nu'}^*w_{\nu'}\right.$$
$$\left.+g_\nu A^*Cu_{\nu'}w_{\nu'}^*-|Cw_{\nu'}|^2\right]+\frac{1}{2}\alpha_2^\nu\left|\frac{B}{t_\nu}\right|^2+\frac{w_\nu}{|s|^2}\alpha_1^\nu\left(\alpha_1^{\mathrm{E}}\alpha_2^{\mathrm{M}}-\alpha_2^{\mathrm{E}}\alpha_1^{\mathrm{M}}\right)^*(A(C^*)^3-A^*|A|^2C^*)$$
$$+\frac{w_{\nu'}}{|s|^2}\alpha_1^{\nu'}\left(\alpha_1^{\mathrm{E}}\alpha_2^{\mathrm{E}}-\alpha_1^{\mathrm{M}}\alpha_2^{\mathrm{M}}\right)^*(A^*|C|^2C^*-(A^*)^3C)\Bigg\}\left(n_2+\frac{1}{2}\right),$$

$$I_7=-\frac{\hbar}{\pi}\int_0^\infty d\omega\frac{4}{3}\omega k^3\sum_{\nu=E,M}\chi_1^\nu\left[2\left|\frac{u_\nu}{s}\right|^2+2\left|\frac{w_\nu}{s}\right|^2+\left|\frac{1}{t_\nu}\right|^2\right]\left(n_1+\frac{1}{2}\right),$$

$$I_8=-\frac{\hbar}{\pi}\int_0^\infty d\omega\frac{8}{3}\omega k^3\sum_{\nu=E,M}\chi_2^\nu\left[\left|\alpha_1^\nu\right|^2\left|A\frac{u_\nu}{s}-g_\nu C\frac{w_\nu}{s}\right|^2+\left|\alpha_1^{\nu'}\right|^2\left|A\frac{w_{\nu'}}{s}+g_\nu C\frac{u_{\nu'}}{s}\right|^2+\frac{1}{2}\left|\frac{\alpha_1^\nu B}{t_\nu}\right|^2\right]\left(n_2+\frac{1}{2}\right),$$

where the definition of the different variables is the same as in Sec. II. In this derivation, we have used the identity

$$\mathrm{Im}\{xy^2\}=2\mathrm{Re}\{xy\}\mathrm{Im}\{y\}+|y|^2\,\mathrm{Im}\{x\}=2\mathrm{Im}\{xy\}\,\mathrm{Re}\{y\}-|y|^2\,\mathrm{Im}\{x\}.$$

Furthermore, the integral over ω' has been carried out using the Dirac δ function of the FDT. After straightforward, lengthy algebraic manipulations, we can rearrange the above terms as

$$\mathcal{P}_1=H_{01}\left[n_0(\omega)-n_1(\omega)\right]+H_{02}\left[n_0(\omega)-n_2(\omega)\right]+H_{21}\left[n_2(\omega)-n_1(\omega)\right], \tag{E1}$$

where

$$H_{01}=\frac{\hbar}{\pi}\sum_{\nu=E,M}\int_0^\infty d\omega 4\omega\chi_1^\nu\Bigg\{\frac{k^3}{3}\left[2\left|\frac{u_\nu}{s}\right|^2+2\left|\frac{w_\nu}{s}\right|^2+\left|\frac{1}{t_\nu}\right|^2\right]-\mathrm{Im}\{\alpha_2^\nu\}\left|A\frac{u_\nu}{s}-g_\nu C\frac{w_\nu}{s}\right|^2$$
$$-\mathrm{Im}\{\alpha_2^{\nu'}\}\left|A\frac{w_\nu}{s}-g_\nu C\frac{u_\nu}{s}\right|^2+\mathrm{Im}\{\alpha_2^\nu A^2\}\left|\frac{u_\nu}{s}\right|^2-\mathrm{Im}\{\alpha_2^\nu C^2\}\left|\frac{w_\nu}{s}\right|^2+2g_\nu\mathrm{Re}\{\alpha_2^\nu AC\}\mathrm{Im}\left\{\frac{u_\nu w_\nu^*}{|s|^2}\right\}$$
$$+\mathrm{Im}\{\alpha_2^{\nu'}A^2\}\left|\frac{w_\nu}{s}\right|^2-\mathrm{Im}\{\alpha_2^{\nu'}C^2\}\left|\frac{u_\nu}{s}\right|^2-2g_\nu\mathrm{Re}\{\alpha_2^{\nu'}AC\}\mathrm{Im}\left\{\frac{u_\nu w_\nu^*}{|s|^2}\right\}+\mathrm{Re}\{\alpha_2^\nu B\}\mathrm{Im}\{B\}\left|\frac{1}{t_\nu}\right|^2\Bigg\},$$

$$H_{02}=\frac{\hbar}{\pi}\sum_{\nu=E,M}\int_0^\infty d\omega\omega\frac{8k^3}{3}\chi_1^\nu\left\{\left|\alpha_2^\nu\right|^2\left|A\frac{u_\nu}{s}-g_\nu C\frac{w_\nu}{s}\right|^2+\left|\alpha_2^{\nu'}\right|^2\left|A\frac{w_\nu}{s}-g_\nu C\frac{u_\nu}{s}\right|^2+\frac{1}{2}\left|\alpha_2^\nu\frac{B}{t_\nu}\right|^2\right\},$$

$$H_{21}=\frac{\hbar}{\pi}\sum_{\nu=E,M}\int_0^\infty d\omega 4\omega\chi_1^\nu\left\{\mathrm{Im}\{\alpha_2^\nu\}\left|A\frac{u_\nu}{s}-g_\nu C\frac{w_\nu}{s}\right|^2+\mathrm{Im}\{\alpha_2^{\nu'}\}\left|A\frac{w_\nu}{s}-g_\nu C\frac{u_\nu}{s}\right|^2+\frac{1}{2}\mathrm{Im}\{\alpha_2^\nu\}\left|\frac{B}{t_\nu}\right|^2\right\}.$$

Finally, Eq. (5) can be readily obtained by reorganizing these expressions.

*a.manjavacas@csic.es
†j.g.deabajo@csic.es

[1]C. M. Hargreaves, Phys. Lett. A **30**, 491 (1969).
[2]G. A. Domoto, R. F. Boehm, and C. L. Tien, J. Heat Transfer **92**, 412 (1970).
[3]D. Polder and M. Van Hove, Phys. Rev. B **4**, 3303 (1971).

[4] A. Narayanaswamy, S. Shen, L. Hu, X. Chen, and G. Chen, Appl. Phys. A **96**, 357 (2009).
[5] R. S. Ottens, V. Quetschke, S. Wise, A. A. Alemi, R. Lundock, G. Mueller, D. H. Reitze, D. B. Tanner, and B. F. Whiting, Phys. Rev. Lett. **107**, 014301 (2011).
[6] J. J. Loomis and H. J. Maris, Phys. Rev. B **50**, 18517 (1994).
[7] R. Carminati and J. J. Greffet, Phys. Rev. Lett. **82**, 1660 (1999).
[8] A. V. Shchegrov, K. Joulain, R. Carminati, and J. J. Greffet, Phys. Rev. Lett. **85**, 1548 (2000).
[9] A. I. Volokitin and B. N. J. Persson, Phys. Rev. B **63**, 205404 (2001).
[10] A. Narayanaswamy and G. Chen, Appl. Phys. Lett. **82**, 3544 (2003).
[11] A. I. Volokitin and B. N. J. Persson, Phys. Rev. B **69**, 045417 (2004).
[12] A. I. Volokitin and B. N. J. Persson, Rev. Mod. Phys. **79**, 1291 (2007).
[13] M. I. Mishchenko, Rev. Geophys. **46**, RG2003 (2008).
[14] S. Basu, Z. M. Zhang, and C. J. Fu, Int. J. Energy Res. **33**, 1203 (2009).
[15] E. Rousseau, A. Siria, G. Jourdan, S. Volz, F. Comin, J. Chevrier, and J. J. Greffet, Nat. Photon. **3**, 514 (2009).
[16] J. P. Mulet, K. Joulain, R. Carminati, and J. J. Greffet, Appl. Phys. Lett. **78**, 2931 (2001).
[17] M. Prunnila and J. Meltaus, Phys. Rev. Lett. **105**, 125501 (2010).
[18] A. W. Rodriguez, O. Ilic, P. Bermel, I. Celanovic, J. D. Joannopoulos, M. Soljačić, and S. G. Johnson, Phys. Rev. Lett. **107**, 114302 (2011).
[19] A. Kittel, W. Müller-Hirsch, J. Parisi, S. A. Biehs, D. Reddig, and M. Holthaus, Phys. Rev. Lett. **95**, 224301 (2005).
[20] S. Shen, A. Narayanaswamy, and G. Chen, Nano Lett. **9**, 2909 (2009).
[21] J. B. Pendry, J. Phys.: Condens. Matter **11**, 6621 (1999).
[22] P. O. Chapuis, M. Laroche, S. Volz, and J. J. Greffet, Phys. Rev. B **77**, 125402 (2008).
[23] M. Krüger, T. Emig, and M. Kardar, Phys. Rev. Lett. **106**, 210404 (2011).
[24] C. Otey and S. Fan, Phys. Rev. B **84**, 245431 (2011).
[25] G. Domingues, S. Volz, K. Joulain, and J. J. Greffet, Phys. Rev. Lett. **94**, 085901 (2005).
[26] A. Narayanaswamy and G. Chen, Phys. Rev. B **77**, 075125 (2008).
[27] P. O. Chapuis, M. Laroche, S. Volz, and J. J. Greffet, Appl. Phys. Lett. **93**, 201906 (2008).
[28] A. Pérez-Madrid, J. M. Rubí, and L. C. Lapas, Phys. Rev. B **77**, 155417 (2008).
[29] A. Pérez-Madrid, L. C. Lapas, and J. M. Rubí, Phys. Rev. Lett. **103**, 048301 (2009).
[30] G. V. Dedkov and A. A. Kyasov, J. Comput. Theor. Nanosci. **7**, 2019 (2010).
[31] R. Messina and M. Antezza, Phys. Rev. A **84**, 042102 (2011).
[32] P. Ben-Abdallah, S. A. Biehs, and K. Joulain, Phys. Rev. Lett. **107**, 114301 (2011).
[33] S. M. Rytov, *Theory of Electric Fluctuations and Thermal Radiation* (Air Force Cambridge Research Center, Bedford, 1959).
[34] A. Manjavacas and F. J. García de Abajo, Phys. Rev. Lett. **105**, 113601 (2010).
[35] H. C. van de Hulst, *Light Scattering by Small Particles* (Dover, New York, 1981).
[36] C. J. Fu and Z. M. Zhang, Int. J. Heat Mass Transf. **49**, 1703 (2006).
[37] S. A. Biehs, E. Rousseau, and J. J. Greffet, Phys. Rev. Lett. **105**, 234301 (2010).
[38] K. Schwab, E. A. Henriksen, J. M. Worlock, and M. L. Roukes, Nature (London) **404**, 974 (2000).
[39] F. J. García de Abajo, Phys. Rev. B **60**, 6086 (1999).